Journal of Applied Polymer Science

Sequential Mixing as Effective Method in the Reduction of Percolation Threshold of Multiwall Carbon Nanotube in Poly(methyl methacrylate)/ High-Density Poly(ethylene)/MWCNT Nanocomposites

Rajat Patra,[1] Supratim Suin,[2] Dipankar Mandal,[1] B. B. Khatua[2]

[1]Department of Physics, Jadavpur University, Kolkata 700032, India

[2]Materials Science Centre, Indian Institute of Technology Kharagpur, Kharagpur 721302, India

Correspondence to: B. B. Khatua (E-mail: khatuabb@matsc.iitkgp.ernet.in) or D. Mandal (E-mail: dipankar@phys.jdvu.ac.in)

ABSTRACT: This work demonstrates sequential heating protocol to be an effective method in the reduction of percolation threshold of multiwall carbon nanotube (MWCNT) in (70/30 w/w) poly(methyl methacrylate) (PMMA)/high-density poly(ethylene) (HDPE)/ MWCNT nanocomposites. Here, the percolation threshold (P_c) value was reduced to 0.08 wt % of MWCNT, which is the lowest among the ever reported values of P_c for the PMMA system. Moreover, a co-continuous morphology of the minor HDPE phase was evident throughout the major PMMA phase in a highly asymmetric composition (70/30 w/w) of the blend constituents. The AC conductivity as well as the dielectric permittivity values were increased with increase in loading of MWCNT in the nanocomposites. The detailed analysis of electrical and morphological properties is discussed in depth in the article. © 2013 Wiley Periodicals, Inc. J. Appl. Polym. Sci. **2014**, *131*, 40235.

KEYWORDS: microscopy; molding; morphology

Received 21 August 2013; accepted 27 November 2013

DOI: 10.1002/app.40235

INTRODUCTION

Immense research interest has been focused on polymer/carbon nanotube (CNT) nanocomposites in the last few decades because of their dramatically improvement in properties relative to neat polymer and to yield multifunctional materials.[1–19] The high aspect ratio of CNTs allows property enhancement at lower concentrations[20] as compared with conventional filler particles such as carbon black or nanoclays. However, to achieve good reinforcing effect from CNTs, two main issues have to be resolved: homogeneous dispersion of CNTs in a matrix polymer and good interfacial interaction between CNTs and the matrix polymer.[21–27] The strong van der Waals attraction originating from their small size and large surface area leads to the CNTs to form aggregated bundles and make it difficult to disperse into the polymer matrix homogeneously.[28] The interaction between polymer and CNTs can be achieved via chemical modification or functionalization, which increases the interfacial adhesion of the CNTs in host polymers leading to the better dispersion of CNTs in the host polymer.[29–31] However, it suffers from surface defects which reduce the conductivity of CNTs.

Various thermoplastics, such as poly(methyl methacrylate) (PMMA),[17] polycarbonate (PC),[19] etc. have been used to prepare polymer/CNT nanocomposites with improved electrical properties. Amongst them, PMMA is of special interest due to its high optical clarity, amorphous nature, and biocompatibility. PMMA/CNT nanocomposites can be used in various fields, such as, electromagnetic interference (EMI) shielding materials,[32–34] transparent conducting films,[35] gas sensors,[36] etc. Considerable research has already been carried out on the electrical properties of PMMA/CNT nanocomposites prepared through different methods.[1–14] For instance, McClory et al.[1] studied the electrical properties of PMMA/multiwall carbon nanotube (MWCNT) nanocomposites prepared by melt mixing and found a DC conductivity of 10^{-7} S cm^{-1} at 1 wt % MWCNT loading. Du et al.[2] followed coagulation technique to prepare PMMA/SWCNT nanocomposites and reported DC conductivity of 2.4×10^{-8} S cm^{-1} at 0.5 wt % single-wall carbon nanotube (SWCNT) loading. Kim et al.[3] reported DC conductivity ≈1 S cm^{-1} at 10 wt % CNT loading in solution casted PMMA/MWCNT nanocomposites with critical exponent value $t = 2.3$. Skakalova et al.[4] used $SOCl_2$ doped highly purified SWCNT to prepare PMMA/ SWCNT nanocomposites by solution casting. A high electrical conductivity (≈10 S cm^{-1}) was obtained at 10 wt % doped SWCNT loading compared with that (≈2 S cm^{-1}) with undoped SWCNT at similar loading. Schmidt et al.[5] obtained DC conductivity ≈ 2×10^{-1} S cm^{-1} at 1.5 wt % CNT loading in solution casted PMMA/MWCNT nanocomposites. Dai et al.[6] prepared

PMMA/SWCNT stretched fiber nanocomposites by solution casting technique. A DC conductivity $\approx 1 \times 10^{-3}$ S cm^{-1} and $\approx 1 \times 10^{-6}$ S cm^{-1} was obtained along the alignment and perpendicular to the alignment, respectively, at 7 wt % SWCNT loading. Weghkowska et al.[7] prepared transparent and conducting PMMA/MWCNT nanocomposites using $SOCl_2$ functionalized highly pure SWCNT and found DC conductivity $\approx 4.7 \times 10^{-1}$ S cm^{-1} at 0.5 wt % CNT loading. Sundaray et al.[8] followed electrospinning technique to prepare PMMA/MWCNT nanocomposites fibers (CNT oriented along the fiber axis) and showed DC conductivity of $\approx 1 \times 10^{-4}$ S cm^{-1} at 1 wt % MWCNT loading. A report by Yuen et al.[9] revealed higher DC conductivity (8×10^{-6} S cm^{-1}) at 0.75 wt % MWCNT loading in *in situ* polymerized PMMA/MWCNT nanocomposites compared with that prepared by the *ex situ* method. Shang et al.[10] studied the electrical properties of the PMMA/MWCNT nanocomposites prepared through microemulsion polymerization and solution casting to study the effect of manufacturing technique on the electrical properties of the nanocomposites. Lahelin et al.[11] followed *in* situ emulsion and emulsion/suspension polymerization methods to prepare PMMA/MWCNT nanocomposites and found a DC conductivity of 1×10^{-5} S cm^{-1} at 3 wt % CNT loading. A higher DC conductivity (5×10^{-6} S cm^{-1}) was obtained in the microemulsion polymerized PMMA/MWCNT nanocomposites compared with that (1×10^{-7} S cm^{-1}) obtained in solution casted nanocomposites at similar loading (5 wt %) of MWCNT. Kim et al.[12] reported a DC conductivity $\approx 5 \times 10^{-4}$ S cm^{-1} in solution blended PMMA/MWCNT nanocomposites thin film at 3 wt % CNT loading. Lee et al.[13] obtained a DC conductivity of 1×10^{-5} S cm^{-1} at 1.5 wt % MWCNT loading in melt-extruded PMMA/SAN/MWCNT nanocomposites. Logakis et al.[14] reported a DC conductivity $\approx 5 \times 10^{-4}$ S cm^{-1} at 1 wt % MWCNT loading in melt-blended PMMA/MWCNT nanocomposites.

Various manufacturing techniques were followed in the polymer nanocomposites to reduce the percolation threshold of the conducting filler in the nanocomposites. Bhagat et al.[15] followed a sequential heating protocol in (70/30 w/w) PP/HDPE/MWCNT nanocomposites. The percolation threshold was achieved at 0.352 wt % of MWCNT in the nanocomposites due to the selective dispersion of MWCNT in the minor HDPE phase. Kim and Jo[16] studied the role of polythiophene-graft-PMMA as a compatibilizer in the poly(styrene-*co*-acrylonitrile) (SAN)/ MWCNT nanocomposites. The incorporation of only 0.01 wt % of MWCNT in SAN matrix in presence of the compatibilizer led to a dramatic increase in both Young's modulus and tensile strength of SAN matrix without sacrificing the inherent elongation at break of SAN. Shrivastava et al.[17] reported an electrical percolation threshold of 0.12 wt % in the PMMA/MWCNT nanocomposites following a method involving the selective dispersion of MWCNT in the *in situ* bulk polymerized PMMA in the presence of PMMA beads. In another work, Shrivastava et al.[18] achieved a percolation threshold of 0.032 wt % of MWCNT in SAN/ MWCNT nanocomposites via exclusion of some portions in the nanocomposites through addition of the SAN beads during *in situ* polymerization of styrene and acrylonitrile in the oligomeric stage. Maiti et al.[19] reported an electrical percolation threshold of 0.14 wt % of MWCNT in polycarbonate (PC)/polycaprolactone (PCL)/MWCNT nanocomposites via melt-dilution of PCL/MWCNT masterbatch with PC. The easy processibilty of PCL favored the dispersion of MWCNT throughout the miscible PC/PCL blend.

Moreover, some authors have used conducting filler in different versatile applications depending on their inherent property. For instance, Wang et al.[37] achieved an electrical conductivity of 2.4×10^7 S m^{-1} in silver nanocrystals based nylon and polyester nanocomposites following sputtering technique. Xu et al.[38] studied the crystallization behavior of poly(trimethylene terephthalate)-poly(ethylene glycol) (PTEG) segmented copolyesters/ MWCNT nanocomposites and found that that MWCNT played the role of an effective nucleating agent during composite crystallization and expedite the process of crystallization of the PTEG matrix by providing more nucleation sites to the crystallizing phase, which resulted in the formation of smaller spherulites. Yang et al.[39] prepared poly(vinyl alcohol) (PVA)/graphene oxide nanocomposites with improved thermal and mechanical properties. The dispersion of graphene oxide on a molecular scale and their alignment in the PVA matrix favors the strong interfacial interactions between both the components, which are responsible for the significant improvement in the thermal and mechanical properties of the nanocomposites.

Despite the above efforts, attainment of electrical conductivity at a significantly low percolation threshold in an easy industrially feasible technique has remained a great deal to date. Here, melt-blending is introduced as an efficient way for the reduction of percolation threshold. This method involves a sequential heating protocol during melt-mixing, where the melt mixing was first carried out at the processing temperature of minor component (HDPE) in the presence of MWCNT for few minutes. Then, the temperature was raised to the processing temperature of the other constituent (PMMA). This protocol did not allow the minor phase to become droplet, and remained as co-continuous. The percolation threshold was reduced to 0.08 wt % of MWCNT, which is, as per our knowledge, the lowest value reported for PMMA/MWCNT system. A co-continuous morphology was obtained in a highly asymmetric composition (70/30) (w/w) PMMA/HDPE. The influence of the processing technique on the morphology and electrical properties of the PMMA/HDPE/MWCNT nanocomposites has been described in detail in the article.

EXPERIMENTAL

Materials Details

General purpose, noncross-linked PMMA (grade: Gujpol-876G with $M_w \approx 105{,}000$, specific gravity 1.19, melt flow index, MFI: 6 g/10 min at 230°C and 1.2 kg load) pellets (average diameter ≈2.35 mm and length ≈2.70 mm) was purchased from Gujarat State Fertilizers and Chemicals Ltd. (GSFC), Gujarat, India. The MWCNT (NC 7000 series; average diameter of 9.5 nm and length 1.5 μm; surface area 250–300 m^2/g; 90% carbon purity) used in the present work was of industrial grade, purchased from Nanocyl S.A., Belgium. The MWCNTs were used as received, without any chemical modifications.

Preparation of the Nanocomposites by Melt Blending

Before the melt blending all the blend constituents (PMMA, HDPE, and MWCNT) were dried in a vacuum oven at 80°C for

6 h to minimize any moisture induced thermal degradation during melt blending. The PMMA, HDPE, and MWCNT were then fed into an internal mixer (Brabender plasticorder with capacity of 20 mL), containing two counter-rotating screws. The composites were prepared by two different methods at various blending compositions (90/10, 80/20, 70/30, and 60/40 w/w) of PMMA and HDPE. In method 1, melt-mixing was done following a sequential heating protocol. First, the temperature of the mixer was maintained at 150°C (above melting temperature of HDPE but well below the melting temperature of PMMA) at 40 rpm for 10 min. Then, the temperature of the internal mixer was gradually increased to 210°C under constant rpm. The mixing was performed at 210°C for 5 min with constant rotor speed (40 rpm). A schematic for method 1 is represented in scheme 1. In method 2, the nanocomposites of similar compositions were prepared by direct melt-blending at a rotor speed of 40 rpm for 15 min. The temperature of mixing was maintained at 210°C throughout the blending time.

Molding of the PMMA/MWCNT Composites

The melt blended PMMA/HDPE/MWCNT composites with various asymmetric blend compositions at various MWCNT loading were compression molded at 210°C for 10 min in a hot press under constant pressure (10 MPa) and the molded parts were allowed to cool to room temperature for further characterizations.

Characterizations

Scanning Electron Microscopic (SEM) Analysis. The degree of dispersion and location of MWCNT in the PMMA/HDPE blend was studied by scanning electron microscope (SEM, VEGA II LSU, TESCAN, Czech Republic) and field emission-scanning electron microscope (Carl Ziess-SUPRATM 40) instruments operated at an accelerating voltage of 10 kV. The cryo-fractured surfaces of the PMMA/HDPE/MWCNT nanocomposites specimens were coated with a thin layer of gold by sputtering to avoid any electrical charging during scanning and SEM micrographs were taken on the fractured surface.

Transmission Electron Microscopy (TEM) Analysis. The state of dispersion of the MWCNT in the (70/30 w/w) (PMMA/HDPE)/MWCNT nanocomposites was studied by transmission electron microscope (HRTEM, JEM-2100, JEOL, Japan) operated at an accelerating voltage of 200 kV. The nanocomposites samples were ultra-microtomed under cryogenic condition with a thickness of 50 to 80 nm. Since the CNT has much higher electron density than the polymers, no staining was required and the CNTs appeared dark in the TEM images.

Differential Scanning Calorimetry Study. A differential scanning calorimeter (DSC-200 PC, NETZSCH, Germany) was employed to determine the nonisothermal crystallization temperature (T_c), and melting temperature (T_m) of the pristine HDPE as well as that in the (70/30, w/w) PMMA/HDPE/nanocomposites at 0.25 wt % MWCNT loading to evaluate the nucleating efficiency of the MWCNT towards HDPE. For this measurement, 10 mg of the vacuum dried sample was taken and heated from room temperature to 150°C at a heating rate of 10°C/min and was kept at 250°C for 10 min to remove previous thermal history. Then, the sample was cooled to room temperature at a cooling rate of 10°C/min to observe the nonisothermal crystallization behavior during cooling. The second heating was carried out to determine the T_m of the respective samples. The heat of crystallization (ΔH_c) and the heat of fusion (ΔH_f) were calculated from the peak area of the melting and second heating curve, respectively.

Measurement of Electrical Conductivity. The measurement of room temperature DC conductivity was carried out on the compression molded specimen bars with dimensions of 30 × 10 × 3 mm^3. A two-probe technique was employed for the measurement of electrical conductivity of the nanocomposites. The nanocomposites samples were fractured at two ends and the fractured surface was coated with silver paste to ensure good contact of the sample surface with the electrodes. Here, the reported DC conductivity values are the averages of at least five tests performed for each sample. The DC conductivity (σ_{DC}) of the composites was calculated from the I-V (current-voltage) measurement using the following relation:

$$\sigma_{DC} = \frac{IL}{VA} \tag{1}$$

where, I is the current measured at the applied voltage V. L and A are the length and cross-sectional area of the sample, respectively.

A computer-controlled LCR Tester (HIOKI 3532-50 LCR HiTESTER, Japan) was used to measure alternating current (AC) conductivity and dielectric properties of the nanocomposites. An alternating electric field (1V) was applied across the sample having diameter of 15 mm and 3 mm thickness in the frequency range of 42 to 10^5 Hz. The parameters like dielectric constant (ε'), dielectric loss (ε''), and dissipation factor (tan δ) were obtained as a function of frequency. All the measurements were carried out at room temperature. The AC conductivity (σ_{AC}) was calculated using the relation:

$$\sigma_{AC} \approx \omega\, \varepsilon_0\, \varepsilon' \tan\delta \tag{2}$$

where, ω is angular frequency of the applied electric field ($\approx 2\pi f$), f is the measured frequency, ε_0 is vacuum permittivity ($\approx 8.854 \times 10^{-12}$ F/m), tan δ is the ratio of ε'' and ε'. The complex permittivity or complex dielectric constant can be calculated using the following equation:

$$\varepsilon' \approx \frac{C_p}{C_0} \tag{3}$$

where, C_p is the observed capacitance of the sample in parallel circuit mode and C_0 is the capacitance of the cell (without dielectric material). C_0 can be calculated by the following relation:

$$C_0 = \frac{\varepsilon_0 A}{d} \tag{4}$$

where, A is area of the capacitor plates ($\approx \pi r^2$) and d is distance between the two capacitor plates (thickness of the sample).

RESULTS AND DISCUSSION

Morphology

The phase morphology of the (70/30, w/w) PMMA/HDPE blend with 0.25 wt % and 1.0 wt % MWCNT prepared through direct mixing (method 2) is shown in Figure 1(a,b), respectively.

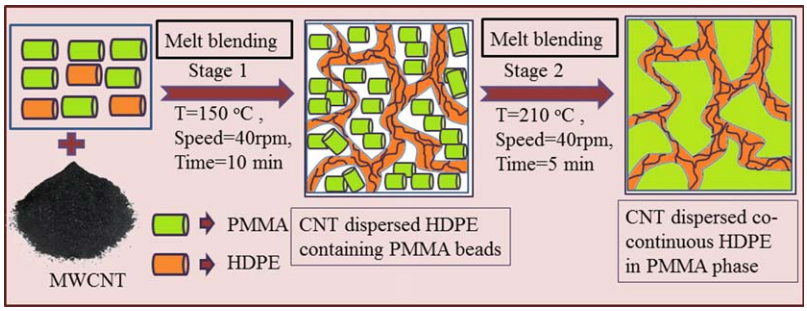

Scheme 1. Sequential heating protocol in method 1 for the preparation of HDPE/PMMA/MWCNT nanocomposites. [Color figure can be viewed in the online issue, which is available at wileyonlinelibrary.com.]

As observed, highly immiscible two phase matrix-droplet morphology was evident at both the lower and higher loading of MWCNT, when the nanocomposites were prepared through the direct blending technique. In general, in immiscible polymer blend of asymmetric composition, the minor component forms the dispersed phase, whereas, the major component forms the continuous matrix and thus resulting matrix droplet morphology in the final nanocomposites. Thus, a PMMA matrix with dispersed HDPE droplet can be concluded in the (70/30, w/w) (PMMA/HDPE)/MWCNT nanocomposites. However, a decrease in droplet size was evident with the increase in MWCNT loading in the nanocomposites, supporting the greater barrier effect coming from the higher loading of MWCNT.

Very surprisingly, the matrix droplet morphology got disappeared with the appearance of highly co-continuous structure of HDPE phase throughout the PMMA matrix when the sequential heating protocol (method 1) was adopted to prepare the nanocomposites. Figure 2(a,b) depict the co-continuous morphology of (70/30 w/w) PMMA/HDPE/MWCNT nanocomposites prepared through method 1. An extensive analysis through the FESEM predicts the presence of MWCNT in the minor HDPE phase [Figure 2(c), inset image is at the higher magnification]. During preparation of the nanocomposites following the sequential heating protocol, at the first stage of mixing at 150°C (above the T_m of HDPE and below the T_m of PMMA), the MWCNTs were dispersed into the molten HDPE, which formed the matrix phase leaving the solid PMMA beads as excluded volume. After 10 min of mixing, the temperature of the mixer was raised to 210°C (above the T_m of both PMMA and HDPE). Under this stage, the major component (PMMA) melted and tends to form the matrix phase. At the same time, the pre-dispersed MWCNTs presented in the HDPE phase restricted the phase inversion, and thus, resulted in the formation of a co-continuous structure (elongated form) rather than the matrix-droplet morphology throughout the composites though PMMA is the major component in this system. All the MWCNTs located in the HDPE phase as the unmodified MWCNT does not have any special affinity (interaction or attraction towards PMMA) to migrate to the PMMA phase during the second stage of processing at high temperature (210°C) in method 1. The interfacial adhesion of two immiscible blends was also improved once co-continuous morphology was formed. Figure 2(d) represents the TEM image of the (70/30, w/w PMMA/HDPE)/MWCNT (0.5 wt %) nanocomposites prepared through method 1. As observed, the MWCNTs were located in the

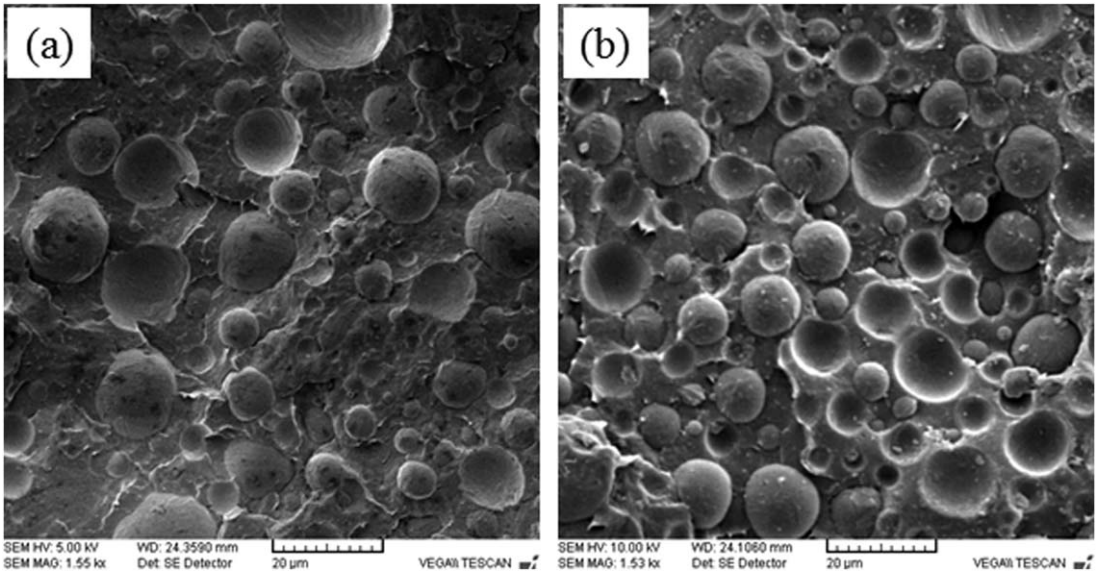

Figure 1. Scanning electron microscopic images of (70/30, w/w) PMMA/HDPE blend/MWCNT nanocomposites prepared through the direct blending (method 2). (a) 0.25 wt %, and (b) 1 wt % MWCNT.

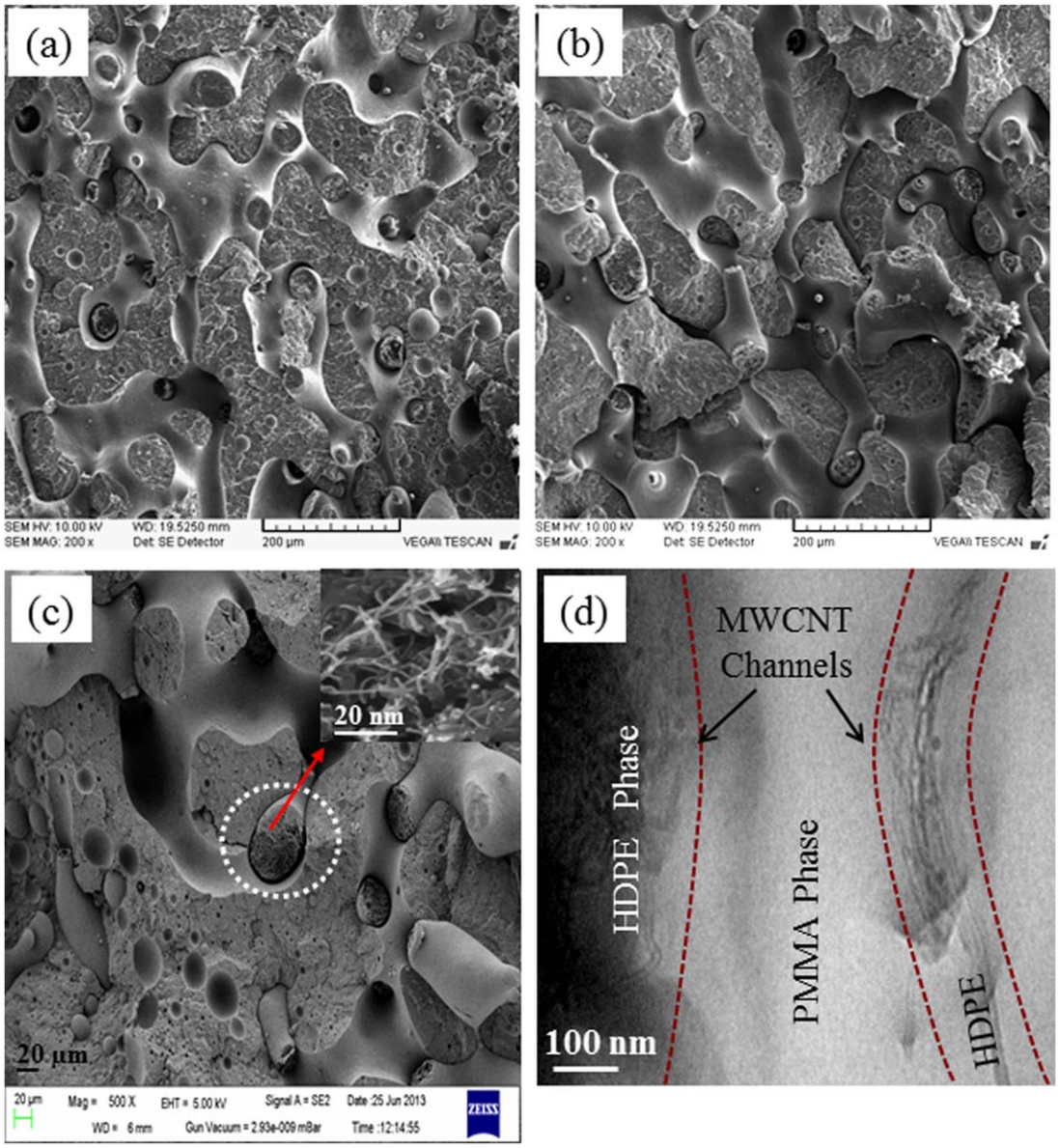

Figure 2. Scanning electron microscopic image with (a) 0.25 wt %, (b) 1 wt % MWCNT; (c) FESEM image at 0.5 wt % MWCNT loading (inset at higher magnification); (d) TEM image at 0.25 wt % MWCNT loading of the (70/30 w/w PMMA/HDPE)/MWCNT nanocomposites prepared by method 1 (sequential heating). [Color figure can be viewed in the online issue, which is available at wileyonlinelibrary.com.]

HDPE phase, forming networks of MWCNTs throughout the composites matrix. This could be because of selective dispersion and distribution of MWCNT in the HDPE phase prior to the melting of PMMA during melt mixing with sequential heating protocol. The presence of MWCNTs in the HDPE phase played the role of physical barrier and prevented the phase inversion of HDPE to become a droplet. The SEM and TEM analysis led us to conclude that, the development of co-continuous morphology in highly asymmetric composition (70/30 w/w) of PMMA/HDPE blend in the presence of MWCNT was because of the sequential heating protocol adopted in method 1.

The favorable dispersion of MWCNT in the HDPE phase rather than the major PMMA phase of the (70/30 w/w) PMMA/HDPE/MWCNT nanocomposites in method 1 might be associated with the high degree of interaction of MWCNT toward HDPE. Such kind of interaction has already been experimentally proven by various groups[40–42] in terms of nucleation effect of MWCNT in HDPE, which in turn affect the T_c, ΔH_c, T_m, and ΔH_f of the HDPE phase in the nanocomposites. Figure 3 represents the DSC cooling [Figure 3(a)] and second heating scans [Figure 3(b)] of the pristine HDPE as well as the (70/30 w/w) PMMA/HDPE/MWCNT nanocomposites containing 0.25 wt % MWCNT. Table I depicts the corresponding numeric data for the T_c, ΔH_c, T_m, and ΔH_m of HDPE in the nanocomposites prepared by method 1. As evident, during cooling the nanocomposites crystallizes at higher temperature (112.26°C) compared with that of the pristine HDPE (108.67°C). The reduction in heat absorbed/released data is also consequent with the nucleating effect of MWCNT toward HDPE.

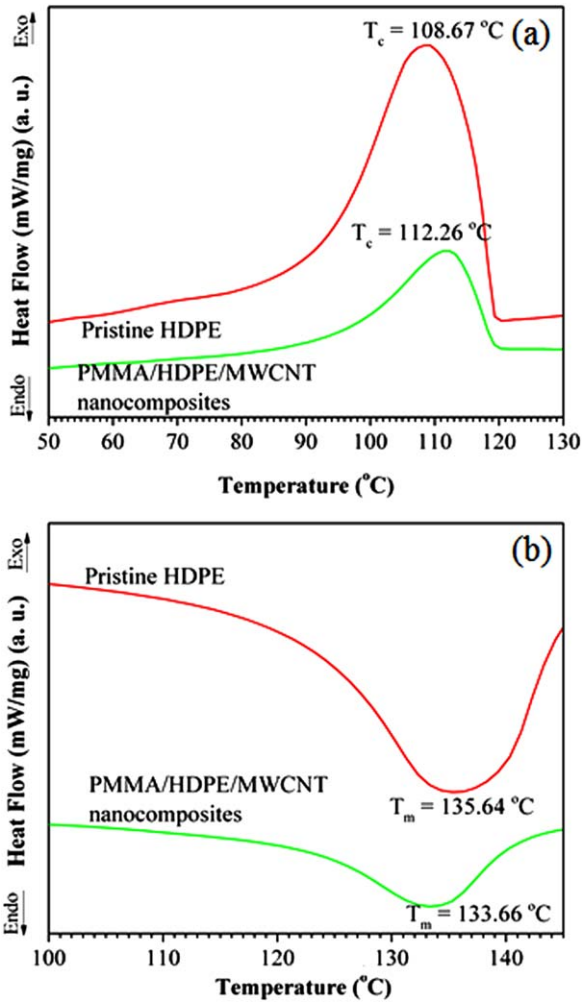

Figure 3. DSC plots for pristine HDPE and PMMA/HDPE/0.25 wt % MWCNT nanocomposites prepared by method 1 during (a) cooling, (b) second heating. [Color figure can be viewed in the online issue, which is available at wileyonlinelibrary.com.]

We also checked the morphology of the blend/MWCNT nanocomposites in other asymmetric ratios (90/10, 80/20, and 60/40 w/w) of PMMA and HDPE in the blend. It was noteworthy; the blend/MWCNT nanocomposites containing 10 wt % and 20 wt % of HDPE did not revealed any co-continuous microstructure irrespective of the mixing methods and MWCNT loading. In all the cases, the nanocomposites exhibited matrix-droplet morphology in the SEM micrograph [Figure 4(a,b)]. However, a co-continuous structure [Figure 4(c)] was observed when the nanocomposites with 40 wt % of HDPE (60/40 w/w PMMA/HDPE) was prepared by method 1 in the presence of small amount (0.25 wt %) of MWCNT.

Electrical Property

The room temperature DC conductivity of the (70/30 w/w) (PMMA/HDPE)/MWCNT (0.25–1.5 wt %) nanocomposites prepared through both the methods is depicted in Figure 5. As observed, the nanocomposites prepared through the method 2 were devoid of any conductivity below 0.75 wt % MWCNT loading. However, a DC conductivity value of 2.53×10^{-4} S cm^{-1} was achieved in the blend/MWCNT nanocomposites at 0.25 wt % loading of MWCNT when the nanocomposites was prepared by employing a sequential heating protocol technique in method 1. A significantly higher value (3.28×10^{-3} S cm^{-1}) of DC conductivity was obtained in the nanocomposites prepared by method 1 at 0.75 wt % loading of MWCNT, as compared with the conductivity value (3.37×10^{-6} S cm^{-1}) of the nanocomposites with similar composition, prepared by the method 2. During sequential heating protocol in method 1, the melt blending was first carried out above the T_m of HDPE (150°C) in the presence of MWCNT. Then, the temperature was raised to the processing temperature of PMMA (210°C) and the mixing was allowed to continue for another 5 min. At the first stage of mixing, the MWCNTs were forced to disperse selectively in the minor HDPE phase of the blend. Further increase in temperature to 210°C could not favor the migration of the MWCNTs to the PMMA phase during the melt mixing. Thus, the effective concentration of MWCNTs in HDPE is almost three times higher in the nanocomposites, as the MWCNTs were dispersed selectively in the 30 wt % HDPE phase. The MWCNT-rich HDPE phase was appeared as co-continuous (fibrillated) form along with the PMMA matrix and thus, formed the effective conductive pathways through the MWCNT-MWCNT network, leading to higher conductivity value. In the direct mixing process, the MWCNTs were present in both the PMMA and HDPE phases, as method 2 did not involve such selective dispersion of MWCNT in the HDPE phase. Thus, the effective concentration of MWCNT in the nanocomposites was similar to that of the MWCNT added during mixing. Moreover, the poor dispersion of the MWCNTs throughout the PMMA matrix resulted in cluster of MWCNT in PMMA phase and was unable to form continuous network structure of MWCNTs. This reduced the number of MWCNT-MWCNT contact points, lacking the formation of efficient network structure, and hence, lowered the conductivity value at similar loading (0.75 wt %) of CNT. The PMMA/HDPE/MWCNT nanocomposites with various amount of MWCNT loading prepared by method 1 (sequential heating protocol) exhibited higher electrical conductivity value compared with the nanocomposites prepared by the method 2 (direct mixing). The selective dispersion of MWCNT in the minor HDPE phase in method 1 might be the possible reason behind the higher electrical conductivity of the nanocomposites prepared in the sequential heating method.

Table I. DSC Result for T_c, ΔH_c, T_m, and ΔH_f for HDPE and (70/30 w/w) (PMMA/HDPE)/0.25 wt % MWCNT Nanocomposites Prepared by Method 1

Sample name	T_c (°C)	ΔH_c (J/g)	T_m (°C)	ΔH_f (J/g)
HDPE	108.67	115.19	135.64	129.28
PMMA/HDPE/MWCNT nanocomposites	112.26	59.48	133.66	57.82

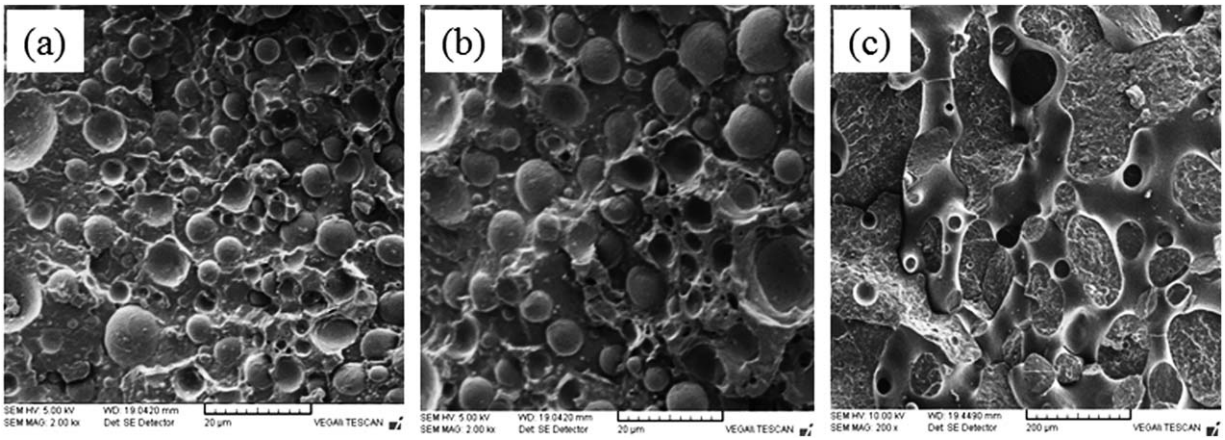

Figure 4. SEM images of (a) (90/10 w/w), (b) (80/20 w/w) (PMMA/HDPE)/MWCNT nanocomposites with 1.5 wt % MWCNT loading, and (c) (60/40 w/w) (PMMA/HDPE)/MWCNT nanocomposites with 0.25 wt % MWCNT loading. All the nanocomposites were prepared by method 1.

To check the composition dependent electrical conductivity, we also investigated the electrical conductivity of the blend/MWCNT nanocomposites at other three asymmetric compositions (90/10, 80/20, and 60/40 w/w) of PMMA and HDPE in the blend. The electrical conductivity of these blend/MWCNT nanocomposites at various MWCNT loadings are represented in Table II. As can be seen, the (90/10 w/w and 80/20 w/w) (PMMA/HDPE)/MWCNT nanocomposites prepared by method 1 (sequential heating) did not exhibit any conductivity up to 1.5 wt % MWCNT loading. This could be due to the absence of any co-continuous structure [Figure 4(a,b)] in these blend compositions in the presence of MWCNT. In both the cases, MWCNT was selectively located in the HDPE phase, which forms the dispersed droplets in the PMMA matrix in the final nanocomposites. Thus, absence of continuous network of MWCNT throughout the matrix phase results in the formation of insulating (PMMA/HDPE)/MWCNT nanocomposites in both these asymmetric blend compositions. However, the blend/MWCNT nanocomposites with (90/10 w/w) and (80/20 w/w) PMMA/HDPE blend compositions showed electrical conductivity at 1.5 wt % and 1 wt % MWCNT loading, respectively, when the nanocomposites were prepared by method 2. Since, method 2 did not involve any selective dispersion of MWCNT in either phase; the MWCNTs were present in both the PMMA and HDPE phases. This leads to the formation of continuous conducting pathways of MWCNT in the nanocomposites at these MWCNT loadings, and hence, becomes conducting in nature.

It is interesting to note that the (60/40 w/w) (PMMA/HDPE)/MWCNT nanocomposites prepared by method 1 showed electrical conductivity even at 0.25 wt % MWCNT loading, similar to that of (70/30 w/w) (PMMA/HDPE)/MWCNT nanocomposites. However, the conductivity value was relatively lower, as compared with that of (70/30 w/w) (PMMA/HDPE)/MWCNT nanocomposites, at similar MWCNT loading. The development of electrical conductivity at low MWCNT loading (0.25 wt %) in this asymmetric blend composition of the nanocomposites, prepared by method 1, could be due to the formation of co-continuous morphology [Figure 4(c)] where the MWCNT-rich HDPE phase formed the effective conductive pathways through the MWCNT-MWCNT network. A relatively low conductivity value in (60/40 w/w) (PMMA/HDPE)/MWCNT nanocomposites compared with that of (70/30 w/w) (PMMA/HDPE)/MWCNT nanocomposites, at similar MWCNT loading, can be explained in terms of selective dispersion of the MWCNT in higher volume of HDPE phase in (60/40 w/w) PMMA/HDPE blend composition.

Figure 6 represents the room temperature DC conductivity of (70/30 w/w) (PMMA/HDPE)/MWCNT nanocomposites with varying amount of MWCNT, prepared by the method 1. An increase in DC conductivity of the (70/30 w/w) (PMMA/HDPE)/MWCNT nanocomposites was evident with increase in MWCNT loading. As observed, the DC conductivity of the nanocomposites suddenly increased up to seven orders (10^7) of magnitude at 0.5 wt % MWCNT loading. This sudden increase in DC conductivity indicates the formation of a percolating path through co-continuous HDPE phase into the (PMMA/

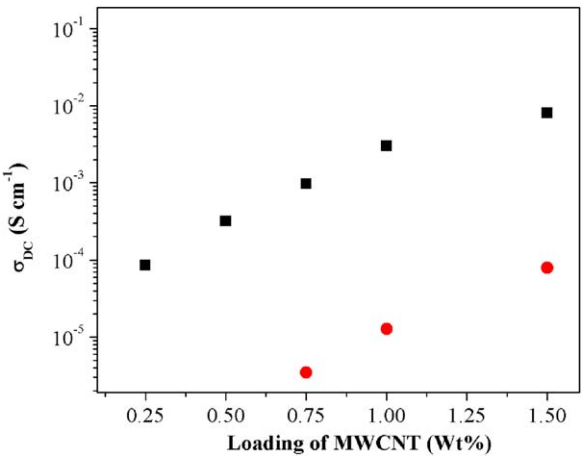

Figure 5. Comparison of DC conductivity at different MWCNT loading for (70/30 w/w) (PMMA/HDPE)/MWCNT nanocomposites prepared by method 1 (■) and method 2 (●). [Color figure can be viewed in the online issue, which is available at wileyonlinelibrary.com.]

Table II. DC Conductivity Values of (90/10, 80/20, and 60/40 w/w) (PMMA/HDPE)/MWCNT Nanocomposites at Different Loadings of MWCNT Prepared Through Method 1 and Method 2

PMMA/HDPE ratio (w/w) MWCNT loading	σ_{DC} (S cm^{-1})					
	90/10		80/20		60/40	
	Method 1	Method 2	Method 1	Method 2	Method 1	Method 2
0.25	-	-	-	-	3.56×10^{-5}	-
0.5	-	-	-	-	8.84×10^{-5}	-
0.75	-	-	-	-	2.48×10^{-4}	5.12×10^{-6}
1	-	-	-	4.8×10^{-6}	6.76×10^{-4}	6.36×10^{-5}
1.5	-	2.14×10^{-6}	-	8.76×10^{-6}	1.16×10^{-4}	9.18×10^{-5}

HDPE)/MWCNT nanocomposites. The exceptionally lower value (0.08 wt %) of percolation threshold (P_c) observed in this work is, to the best of our knowledge, the lowest value reported till date for the PMMA/MWCNT composites systems. Above the P_c, the bulk conductivity of the composites is related with the scaling law, as presented in the eq. (5).[32–36]

$$\sigma_{DC} \propto (P - P_c)^t \quad \text{For}, P > P_c \tag{5}$$

where, σ_{DC} is the conductivity of the composites, P is the mass fraction of the filler, P_c is percolation threshold, and t is the critical exponent which is related to the dimensionality of the percolated network. For two-dimensional (2D) network t varies between 1.1 and 1.3[43] and that in a 3D network it varies between 1.6 and 2.0.[44] The 3D percolation theory suggests that the higher critical exponent values (t) compared with the predicted universal value indicates that the percolation is associated with a networks involving less amount of "dead ends." The theory also suggests that the increase in number of "dead ends" decreases the t values in a network. The best fitted straight line was obtained by considering the value for $p_c \approx 0.08$ wt % in the log σ_{DC} versus log($p - p_c$), as shown in the inset of Figure 6.

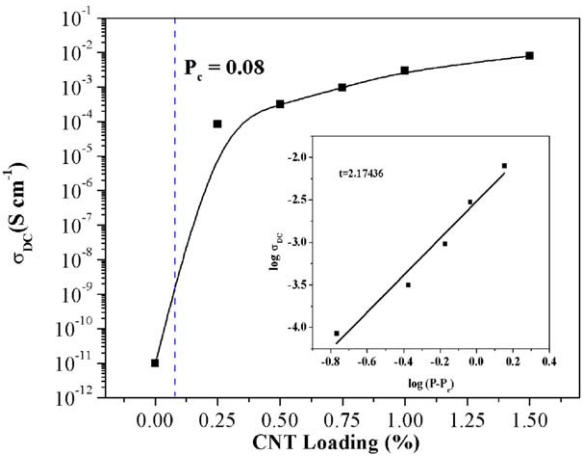

Figure 6. DC conductivity of (70/30 w/w) (PMMA/HDPE)/MWCNT nanocomposites prepared by method 1 as a function of MWCNT loading (p). The inset shows a plot of logσ_{DC} versus log($p - pc$) for the same composites and the straight line represents the best-fitted line of the data to eq. (4), giving best-fit values $p_c \approx 0.08$ and $t \approx 2.17436$. [Color figure can be viewed in the online issue, which is available at wileyonlinelibrary.com.]

The value of t was determined from the slope of log σ_{DC} versus log($p - p_c$) and was found to be 2.17436 with a standard deviation of 0.21364. This result well agrees with the percolation behavior given in eq. (5) and indicates an exceptionally low percolation threshold of 0.08 wt % MWCNT loading in the composites matrix resulting from the excellent dispersion and individualization of high aspect ratio MWCNTs in the matrix. The value of $t \approx 2.17436$ for the CNT composites is well consistent with the theoretically predicted value of $t \approx 2.0$ for a 3D percolation network.[46] As the critical exponent t value is dependent on the microstructural properties (viz. length and diameter of CNTs, carbon purity, structure etc.) of the composites, various researchers have found different t values. The extrapolation of $p \rightarrow 100$ in eq. (5) gives a conductivity of 8.07×10^{-2} S cm^{-1}, which is considerably lower than the reported conductivity value (50 S cm^{-1}) of pure MWCNTs.[47–49] The decrease in conductivity in the PMMA/MWCNT nanocomposites can be explained in terms of coating of insulating polymer over individual nanotubes, resulting in poor electrical contact between the nanotubes and thus generating a large contact resistance.[50]

In general, the energy barrier between the nanotubes restricts the electron transfer from one electrode to another due to the existence of the insulating polymer between them. However, when voltage is applied the shape of the energy barrier gets changed and the electrons between two sufficiently close electrode can move across the barrier via tunneling, resulting in a small current flow. The electrons in the polymer composites tunnel one by one from one MWCNT electrode to the nearest MWCNT electrode through the formation of an MWCNT−polymer pathway. This induces resistance and limits the conductivity of the composites up to a certain limit. The existence of tunneling conduction in polymer−CNT nanocomposites has already been mentioned in the literature.[51,52] With increase in the barrier gap, the conductivity of the nanocomposites rapidly decreases. The tunneling assisted conduction can be expressed in terms of σ_{DC} with the following equation:

$$\sigma_{DC} \propto \exp(-AD) \tag{6}$$

where, A and d represent the tunnel parameter and tunnel distance, respectively. In case the particles are randomly

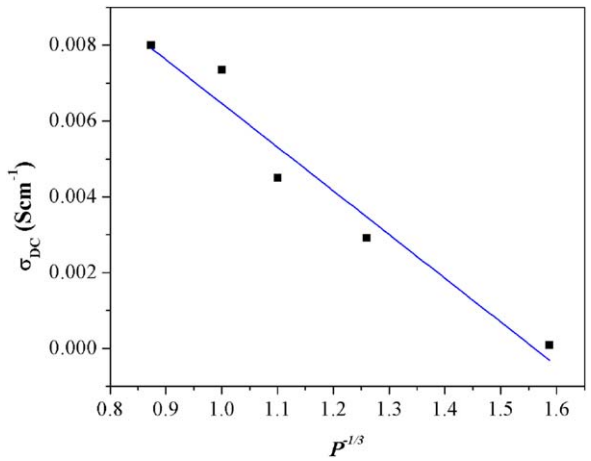

Figure 7. Linear variation of σ_{DC} versus $p-1/3$. [Color figure can be viewed in the online issue, which is available at wileyonlinelibrary.com.]

distributed, the mean average distance (d) among particles can be assumed to be proportional to $P^{-1/3}$. Thus, eq. (6) can be written as,

$$\log(\sigma_{DC}) \propto P^{-1/3} \tag{7}$$

The uniform dispersion of MWCNT in polymer matrix leads to a good anchoring between polymer and CNT, but it suffers from direct contacts between MWCNTs. These results are responsible for the relatively low increment of conductivity above 0.5% CNT loading. In an insulator matrix, a tunneling conductive mechanism is expected to occur in the nanocomposites. The relationship between σ_{DC} and $P^{-1/3}$ is given in eq. (7) and the results are plotted in Figure 7 indicating the presence of tunneling conduction in the nanocomposites.

A drastic change in the DC conductivity (from 10^{-11} to 10^{-4} S cm^{-1}) in the (70/30 w/w) (PMMA/HDPE)/MWCNT composites was obtained in the range of CNT loading 0.01 to 0.35 wt %. The incorporation of higher amount (0.5–1.5 wt %) of CNT showed a stable conductivity in the composites at around 10^{-3} S cm^{-1}, which is an appreciably higher value of conductivity

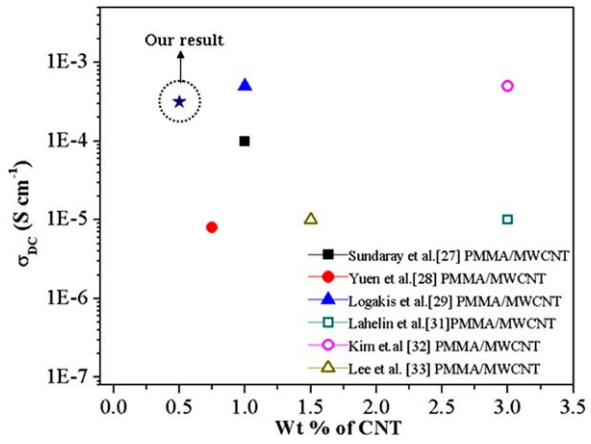

Figure 8. Comparison of our result with published electrical conductivity data for PMMA/MWCNT composites. [Color figure can be viewed in the online issue, which is available at wileyonlinelibrary.com.]

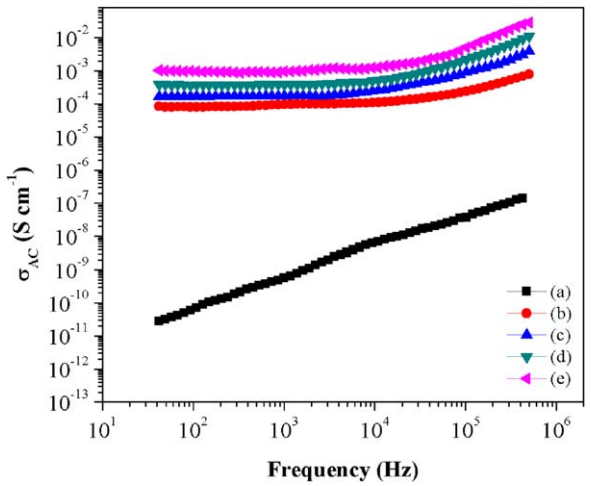

Figure 9. Room temperature AC conductivity as a function of frequency for (a) (70/30 w/w) PMMA/HDPE blend and its nanocomposites with (b) 0.25 wt %, (c) 0.5 wt %, (d) 1 wt %, (e) 1.5 wt % MWCNT, prepared by method 1. [Color figure can be viewed in the online issue, which is available at wileyonlinelibrary.com.]

for PMMA/MWCNT composites at this low level of MWCNT loading, using unaligned, unmodified, commercially available MWCNT.

A comparative study of the conductivity of the (70/30 w/w) (PMMA/HDPE)/MWCNT composites with that of the published data[8,9,20,21,38,39] for PMMA/CNT composites is depicted in Figure 8. The sequential heating protocol (method 1) adopted in our study showed the highest conductivity at the lowest CNT loading compared with the other reported data at such a low level of CNT loading. Such high level of conductivity at such a low loading of MWCNT can be attributed to the conducting CNT filled HDPE channels throughout the PMMA matrix, leaving a large volume of matrix phase as excluded volume.

Figure 9 represents the variation of room temperature AC conductivity of (70/30 w/w) (PMMA/HDPE)/MWCNT nanocomposites prepared through the sequential heating protocol (method 1) with various amounts of MWCNT (0.25, 0.5, 1, and 1.5 wt %) in the frequency range 42 Hz to 5 MHz. As observed, the AC conductivity of nanocomposites was increased with increase in the MWCNT loading. Moreover, the (70/30 w/w) PMMA/HDPE blend showed a gradual increase in conductivity with frequency obeying the typical behavior of an insulating material. A very drastic change in the AC conductivity was observed at lower frequency when 0.25 wt % MWCNT was incorporated in the pure PMMA/HDPE blend. However, addition of more amount of MWCNT did not give rise to a large increment in AC conductivity in the entire range of frequency. These results are indicative to the fact that the percolation threshold has been achieved below 0.25 wt % loading of MWCNT through the formation of more number of network paths of CNTs in the co-continuous HDPE phase. The increase in MWCNT loading in the (PMMA/HDPE)/MWCNT nanocomposites revealed a DC plateau (DC conductivity) up to which the conductivity remains independent of frequency and beyond which the conductivity increases with increase in

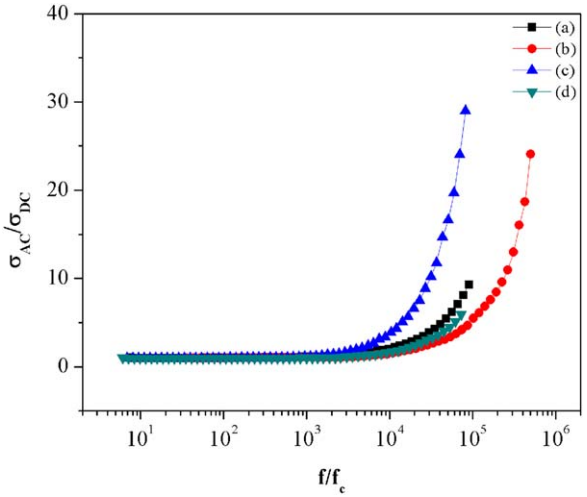

Figure 10. Master curve σ_{AC}/σ_{DC} as a function of f/f_c for the (70/30 w/w) (PMMA/HDPE)/MWCNT nanocomposites prepared by method 1 with (a) 0.25 wt %, (b) 0.5 wt %, (c) 1 wt %, (d) 1.5 wt % MWCNT loadings. [Color figure can be viewed in the online issue, which is available at wileyonlinelibrary.com.]

frequency. At low frequency region, the σ_{AC} of any dielectric material (below f_c) can be expressed in terms of σ_{DC}, $\omega(\approx 2\pi f)$, and ε'' with the following relation:

$$\sigma_{AC} = \sigma_{DC} + \omega\varepsilon'' \tag{8}$$

The first component σ_{DC} of eq. (8) is related to the ionic or electronic conductivity. The second term ($\omega\varepsilon''$) is strongly dependent on the extent of polarization of the permanent as well as the induced dipoles and the charges accumulated at the interface is well known as Maxwell-Wagner-Sillars effect. Below f_c, the dipoles/induced dipoles get sufficient time to orient themselves with the direction of applied electric field and thus, the value of σ_{AC} for a conductive system actually represents the σ_{DC}.

At higher frequency region (above f_c), the polarization effect becomes insignificant as the dipoles get much less relaxation time to orient themselves in the direction of applied electric field. Above f_c, the applied AC electric field restricts the accumulation and dispersion of dipoles in the direction of applied field and reduces the value of polarization. Thus, the value of σ_{AC} is strongly dependent on the excitation of the charge particles and flow of electrons through the continuous conductive network structure in the matrix phase. It is noteworthy that, the critical frequency (f_c) value was shifted to higher region with increase in the loading of MWCNT, supporting the results reported in the literature.[43] This result can be associated with the increase in effective loading of MWCNT in HDPE phase, resulting in more number of effective network channels of the MWCNTs throughout the PMMA phase.

Linares et al.[52] established a relation between AC conductivity and frequency at different concentration of conducting filler. This universal dynamic response[53] can be described as follows:

$$\sigma_{AC} \propto f^s \tag{9}$$

where f is the frequency and s is the s-exponent value which varies between $0 < s < 1$ and the eq. (9) has been considered as universal for heterogeneous system.[54] The value of s-exponent is related to the filler concentration in nanocomposites. Therefore, it is necessary to check under which condition the proposed equation is valid for nanocomposites. In another report Connor et al.[55] reported the conductivity curve for conducting filler filed polymer nanocomposite, which was independent of the concentration (P) of conducting particles. In this case, the curve depends only on DC conductivity and critical frequency. In order to construct a P-independent master curve, the conductivity and frequency were normalized by σ_{DC} and f_c values. Figure 10 shows the master curve for the nanocomposites containing concentration of MWCNT $P > P_c$. By plotting σ_{AC}/σ_{DC} versus f/f_c the conductivity data falls on almost one single curve showing good agreement to their report.

The variation of room temperature dielectric constant (ε') with frequency of (70/30 w/w) PMMA/HDPE blends as well as the blend/MWCNT nanocomposites prepared by method 1, with various amounts of MWCNT is shown in Figure 11. As can be seen, the PMMA/HDPE blend in the absence of MWCNT indicated a nearly constant value (ε'), independent of frequency in the entire frequency range (42–105 Hz). However, a gradual decrease in the value of dielectric constant with increase in frequency was evident in the case of (70/30 w/w) (PMMA/HDPE)/MWCNT nanocomposites, irrespective of the MWCNT content. A relatively higher value of dielectric constant at lower frequency region for (PMMA/HDPE)/MWCNT nanocomposites can be explained in terms of the presence of all types of polarization at room temperature. A slight decrease in dielectric constant with the increase in frequency might be associated with the electronic polarization that dominates at higher frequency, and interfacial dipoles experienced less time to orient themselves in the direction of the alternating field. Above the P_c, the dielectric constant was increased drastically with the increase in MWCNT content for all the (PMMA/HDPE)/MWCNT nanocomposites, consistent with the reported[54,55] results for polymer

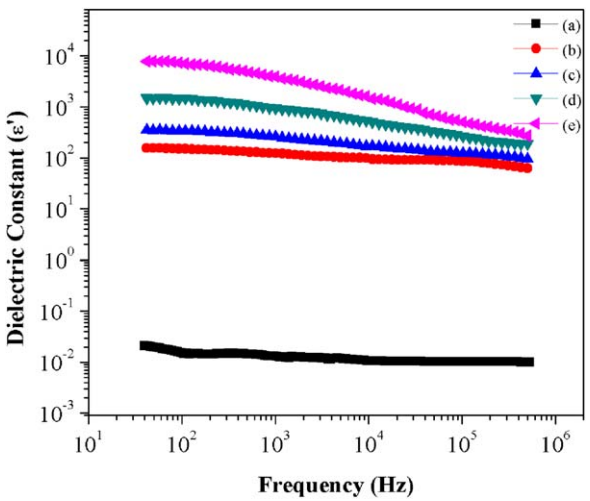

Figure 11. Dielectric constant as a function of frequency for (a) (70/30 w/w) PMMA/HDPE blend and its nanocomposites with (b) 0.25 wt %, (c) 0.5 wt %, (d) 1 wt %, (e) 1.5 wt % MWCNT, prepared by method 1. [Color figure can be viewed in the online issue, which is available at wileyonlinelibrary.com.]

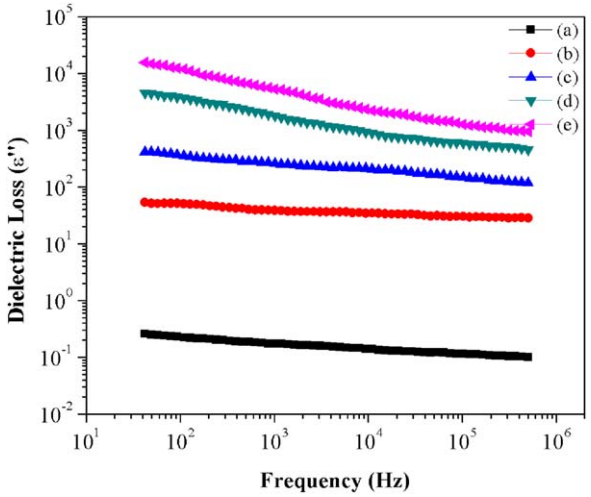

Figure 12. Dielectric loss as a function of frequency for (a) (70/30 w/w) PMMA/HDPE blend and its nanocomposites with (b) 0.25 wt %, (c) 0.5 wt %, (d) 1 wt %, (e) 1.5 wt % MWCNT loadings, prepared by method 1. [Color figure can be viewed in the online issue, which is available at wileyonlinelibrary.com.]

composites containing CB. At low frequencies, the very high values of dielectric constant for the (PMMA/HDPE)/MWCNT nanocomposites above the P_c could be associated with the higher concentration of MWCNT, which increased the number of "dead ends," and generated microcapacitors of various length scales. The charge between the polymer and CNT increased the number of "dead ends" and thus, results in an enhancement in the overall capacitance, which in turn increased the dielectric constant of the nanocomposites.

The room temperature variation in dielectric loss (ε'') with frequency for the (70/30 w/w) (PMMA/HDPE)/MWCNT composites with varying amount of MWCNT is plotted in Figure 12. A decrease in dielectric loss with the increase in frequency was evident in all the nanocomposites under consideration. This behavior may be attributed to the relaxation among dipoles, which cannot be in phase with the frequency of the applied electric field. Moreover, the dielectric loss (ε'') of the nanocomposites was increased with increase in CNT loading. The effect of CNT loading on dielectric loss was more prominent in the lower frequency region, along with a marginal effect at higher frequency. The literature also suggests that, with increase in conducting filler loading dielectric loss increases at lower frequency, supporting our findings.[36]

CONCLUSIONS

Electrical conductivity of (PMMA/HDPE)/MWCNT nanocomposites with various asymmetric blending compositions of PMMA and HDPE, prepared by conventional melt-mixing method adopting sequential heating protocol has been studied in detail. The (PMMA/HDPE)/MWCNT nanocomposites with a blend ratio of (70/30 w/w) PMMA/HDPE revealed significantly higher conductivity value at very low loading of MWCNT compared with the other compositions of the blend in the nanocomposites prepared by sequential heating protocol during melt-mixing (method 1). The morphological analysis revealed a co-continuous morphology in a highly asymmetric composition of the blend constituents arising from the barrier effect of the incorporated MWCNT. The electrical conductivity measurement revealed that electrical conductivity was increased with increase in loading of MWCNT into the PMMA/HDPE/MWCNT nanocomposites. Moreover, the tunneling mechanism was appeared to be responsible for electron conduction in the polymer nanocomposites, suggesting a coating of thin layer of polymer over individual MWCNT. The dielectric result revealed that both the dielectric permittivity and dielectric loss were increased with the increase in MWCNT loading in the nanocomposites.

REFERENCES

1. McClory, C.; Nally, T. M.; Baxendale, M.; Potschke, P.; Blau, W.; Ruether, M. *Eur. Polym. J.* **2010**, *46*, 854.
2. Du, F.; Fischer, J. E.; Winey, K. I. *Phys. Rev. B* **2005**, *72*, 121404.
3. Kim, H. M.; Choi, M. S.; Joo, J.; Cho, S. J.; Yoon, H. S. *Phys. Rev. B* **2006**, *74*, 054202.
4. Skakalova, V.; Weglikowska, U. D.; Roth, S. *Synth. Met.*, **2005**, *152*, 349.
5. Schmidt, R. H.; Kinloch, I. A.; Burgess, A. N.; Windle, A. H. *Langmuir* **2007**, *23*, 5707.
6. Dai, J.; Wang, Q.; Li, W.; Wei, Z.; Xu, G. *Mater. Lett.* **2007**, *61*, 27.
7. Weghkowska, U. D.; Kaempgen, M.; Hornboste, B.; Skakalova, V.; Wang, J.; Liang, J; Roth, S. *Phys. Status Solid. b*, **2006**, *243*, 3440.
8. Sundaray, B.; Subramanian, V.; Natarajana, T. S. *Appl. Phys. Lett.* **2006**, *88*, 143114.
9. Yuen, S. M.; Ma, C. C. M.; Chuang, C. Y.; Yu, K. C.; Wu, S. Y.; Yang, C. C.; Wei, M. H. *Compos. Sci. Technol.* **2008**, *68*, 963.
10. Shang, S.; Li, L.; Yang, X.; Wei, Y. *Compos. Sci. Technol.* **2009**, *69*, 1156.
11. Lahelin, M.; Annala, M.; Nykanen, A.; Ruokolainen, J.; Seppala, J. *Compos. Sci. Technol.* **2011**, *71*, 900.
12. Kim, K. S.; Park, S. *J. Synth. Met.* **2010**, *160*, 123.
13. Lee, M.; Jeon, H.; Min, B. H.; Kim, J. H. *J. Appl. Polym. Sci.*, **2011**, *121*, 743.
14. Logakis, E.; Pandis, C.; Pissis, P.; Pionteck, J.; Potschke, P. *Compos. Sci. Technol.* **2011**, *71*, 854.
15. Bhagat, N. A.; Shrivastava, N. K.; Suin, S.; Maiti, S.; Khatua, B. B. *Polym. Compos.* **2013**, *34*, 787.
16. Kim, K. H.; Jo, W. H. *Macromolecules* **2007**, *40*, 3708.
17. Shrivastava, N. K.; Kar, P.; Maiti, S.; Khatua, B. B. *Polym. Int.* **2012**, *61*, 1683.
18. Shrivastava, N. K.; Suin, S.; Maiti, S.; Khatua B. B. *Ind. Eng. Chem. Res.* **2013**, *52*, 2858.
19. Maiti, S.; Suin, S.; Shrivastava, N. K.; Khatua B. B. *Polym. Eng. Sci.*, **2013**, *165*, 40.
20. Andrews, R.; Jacques, D.; Minot, M.; Rantell, T. *Macromol. Mater. Eng.* **2002**, *287*, 395.

21. Blond, D.; Barron, V.; Ruether, M.; Ryan, K. P.; Nicolosi, V.; Blau, W. J.; Coleman, J. N. *Adv. Funct. Mater.* **2006**, *16*, 1608.
22. Bellayer, S.; Gilman, J. W.; Eidelman, N.; Bourbigot, S.; Flambard, X.; Fox, D. M.; De Long, H. C.; Trulove, P. C. *Adv. Funct. Mater.* **2005**, *15*, 910.
23. Liu, L.; Barber, A. H.; Nuriel, S.; Wagner, H. D. *Adv. Funct. Mater.* **2005**, *15*, 975.
24. Hwang, G. L.; Shieh, Y. T.; Hwang, K. C. *Adv. Funct. Mater.* **2004**, *14*, 487.
25. Coleman, J. N.; Cadek, M.; Blake, R.; Nicolosi, V.; Ryan, K. P.; Belton, C.; Fonseca, A.; Nagy, J. B.; Gunko, Y. K.; Blau, W. *J. Adv. Funct. Mater.* **2004**, *14*, 791.
26. Wang, M.; Pramoda, K. P.; Goh, S. H. *Polymer* **2005**, *46*, 11510.
27. Zhang, X.; Liu, T.; Sreekumar, T. V.; Kumar, S.; Moore V. C.; Hauge, R. H.; Smalley, R. E. *Nano Lett.* **2003**, *3*, 1285.
28. Sahoo, N. G.; Rana, S.; Cho, J. W.; Li, L.; Chan, S. H. *Prog. Polym. Sci.* **2010**, *35*, 837.
29. Hatui, G.; Das, C. K. *J. Polym. Res.* **2013**, *20*, 77.
30. Nayak, G. C.; Rajasekar, R.; Das C. K. *J. Mater. Sci.* **2011**, *46*, 2050.
31. Mukherjee, M.; Nayak, G. C.; Bose, S.; Das C. K. *Polym. Plast. Technol. Eng.* **2009**, *48*, 1107.
32. Kim, H. M.; Kim, K.; Lee, C. Y.; Joo, J.; Cho, S. J.; Yoon, H. S.; Pejakovic, D. A.; Yoo, J. W.; Epstein, A. *J. Appl. Phys. Lett.* **2004**, *84*, 589.
33. Yuen, S. M.; Ma, C. C. M.; Chuang, C. Y.; Yu, K. C.; Wu, S. Y.; Yang, C. C.; Wei, M. H. *Compos. Sci. Technol.* **2008**, *68*, 963.
34. Huang, Y. L.; Yuen, S. M.; Ma, C. C. M; Chuang, C. Y.; Yu, K. C.; Teng, C. C.; Tien, H. W.; Chiu, Y. C.; Wu, S. Y.; Liao, S. H.; Weng, F. B. *Compos. Sci. Technol.* **2009**, *69*, 1991.
35. Kim, D. O.; Lee, M. H.; Lee, J. H.; Lee, T. W.; Kim, K. J.; Lee, Y. K.; Kim, T.; Choi, H. R.; Koo, J. C.; Nam, J. D. *Org. Electron.* **2008**, *9*, 1.
36. Li, Y.; Wang, X. C.; Yang, M. *J. Sens. Actuators B* **2007**, *121*, 496.
37. Wang, R. X.; Tao, X. M.; Wang, Y.; Wang, G. F.; Shang, S. M. *Surf. Coat. Technol.* **2010**, *204*, 1206.
38. Xu, Y.; Shang, S.; Huang, J. *Polym. Test.* **2010**, *29*, 1007.
39. Yang, X.; Shang, S.; Li, L. *J. Appl. Polym. Sci.* **2011**, *120*, 1355.
40. Trujillo, M.; Arnal, M. L.; Mu1ller, A. J.; Bredeau, St.; Bonduel, D.; Dubois, Ph.; Hamley, I. W.; Castelletto, V. *Macromolecules* **2008**, *41*, 2087.
41. Vega, J. F.; Martınez-Salazar, J.; Trujillo, M.; Arnal, M. L.; Muller A. J.; Bredeau, S.; Dubois, Ph. *Macromolecules* **2009**, *42*, 4719.
42. Trujillo, M.; Arnal, M. L.; Mu1ller, A. J.; E. Laredo, Bredeau, St.; Bonduel, D.; Dubois, Ph. *Macromolecules* **2007**, *40*, 6268.
43. Lux, F. *J. Mater. Sci.* **1993**, *28*, 285.
44. Laredo, E.; Prutsky, N.; Bello, A.; Grimau, M.; Castillo, R. V.; Muller, A. J.; Dubois, P. *Eur. Phys. J.* **2007**, *23*, 295.
45. Adler, J.; Meir, Y.; Aharony, A.; Harris, A. B.; Klein, L. *J. Stat. Phys.* **1990**, *58*, 511.
46. Wu, T. M.; Chen, E. C. *Compos. Sci. Technol.* **2008**, *68*, 2254.
47. Fan, J.; Wan, M.; Zhu, D.; Chang, B.; Pan, Z.; Xie, S. *J. Appl. Polym. Sci.* **1999**, *74*, 2605.
48. Barrau, S.; Demont, P.; Peigney, A.; Laurent C.; Lacabanne C. *Macromolecules* **2003**, *36*, 5187.
49. Jonscher, A. K. *Nature* **1977**, *267*, 673.
50. Kilbride, B. E.; Coleman, J. N.; Fraysse, J.; Fournet, P.; Cadek, M.; Drury, A.; Hutzler, S.; Roth, S.; Blau, W. J. *J. Appl. Phys.* **2002**, *92*, 4024.
51. Nanda, M.; Chaudhary, R. N. P.; Tripathy, D. K. *Polym. Compos.* **2010**, *31*, 152.
52. Linares, A.; Canalda, J. C.; Cagiao, M. E.; Garcıa-Gutierrez, M. C.; Nogales, A.; Martın-Gullon, I.; Vera, J.; Ezquerra, T. A. *Macromolecules* **2008**, *41*, 7090.
53. Mahapatra, S. P.; Sridhar, V.; Tripathy, D. K. *J. Appl. Polym. Sci.* **2007**, *106*, 192.
54. Dyre, J. C.; Schroder, T. B. *Rev. Mod. Phys.* **2000**, *72*, 873.
55. Connor, M. T.; Roy, S.; Ezquerra, T. A.; BaltaCalleja, F. *J. Phys. Rev. B* **1998**, *57*, 2286.